JACS
JOURNAL OF THE AMERICAN CHEMICAL SOCIETY

Article

pubs.acs.org/JACS

Enantioselective Polymerization of Epoxides Using Biaryl-Linked Bimetallic Cobalt Catalysts: A Mechanistic Study

Syud M. Ahmed,[†] Albert Poater,[‡,§] M. Ian Childers,[†] Peter C. B. Widger,[†] Anne M. LaPointe,[†] Emil B. Lobkovsky,[†] Geoffrey W. Coates,*[,†] and Luigi Cavallo*[,§]

[†]Department of Chemistry and Chemical Biology, Baker Laboratory, Cornell University, Ithaca, New York 14853-1301, United States,

[‡]Institut de Química Computacional i Catàlisi and Department de Química, Universitat de Girona, Campus de Motilivi, E-17071 Girona, Spain

[§]KAUST Catalysis Center, Chemical and Life Sciences and Engineering, King Abdullah University of Science and Technology, Thuwal 23955-6900, Saudi Arabia

Supporting Information

ABSTRACT: The enantioselective polymerization of propylene oxide (PO) using biaryl-linked bimetallic salen Co catalysts was investigated experimentally and theoretically. Five key aspects of this catalytic system were examined: (1) the structural features of the catalyst, (2) the regio- and stereoselectivity of the chain-growth step, (3) the probable oxidation and electronic state of Co during the polymerization, (4) the role of the cocatalyst, and (5) the mechanism of monomer enchainment. Several important insights were revealed. First, density functional theory (DFT) calculations provided detailed structural information regarding the regio- and stereoselective chain-growth step. Specifically, the absolute stereochemistry of the binaphthol linker determines the enantiomer preference in the polymerization, and the interaction between the salen ligand and the growing polymer chain is a fundamental aspect of enantioselectivity. Second, a new bimetallic catalyst with a conformationally flexible biphenol linker was synthesized and found to enantioselectively polymerize PO, though with lower enantioselectivity than the binaphthol linked catalysts. Third, DFT calculations revealed that the active form of the catalyst has two active *exo* anionic ligands (chloride or carboxylate) and an *endo* polymer alkoxide which can ring-open an adjacent cobalt-coordinated epoxide. Fourth, calculations showed that initiation is favored by an *endo* chloride ligand, while propagation is favored by the presence of two *exo* carboxylate ligands.

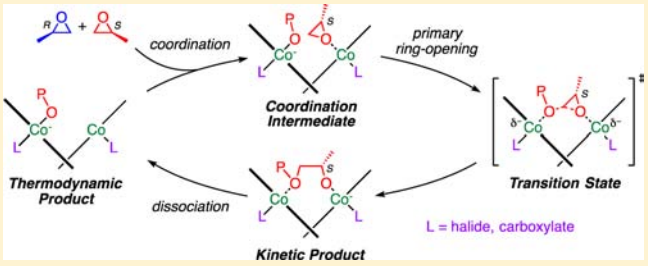

INTRODUCTION

Commercial polyethers are synthesized from readily available racemic epoxides. The catalysts used randomly incorporate both enantiomers into the polymer chain, resulting in atactic and therefore amorphous polyethers. In contrast, many isotactic polyethers are semicrystalline thermoplastics, which increases their range of possible applications. There are two predominant routes to isotactic polyepoxides: (1) polymerization of optically active epoxides and (2) stereoselective polymerization of racemic epoxides. Given the high cost of enantiopure epoxides, the first approach is not economically viable for large-scale production, and until recently, stereoselective catalysts for epoxide polymerization[1] either exhibited low levels of selectivity and/or activity[2] or were heterogeneous mixtures that produced a combination of isotactic and atactic polymer chains.[3]

In 2005, we reported a cobalt salen catalyst, **1** (Scheme 1), that is highly active and isoselective for the polymerization of racemic propylene oxide (PO), to yield isotactic poly(propylene oxide) (PPO) with an *mm*-triad content of >99%.[4] Complex **1** is limited in substrate scope, though it isoselectively polymerizes PO and butene oxide in high yields. Given the unexpected isotacticity of the polymer formed using this achiral catalyst, a series of mechanistic studies were performed to determine the origin of isotacticity. X-ray analysis of a single crystal of the methoxide derivative, **2**, which is also isoselective, showed the presence of chiral clefts that are postulated to be responsible for the stereocontrol through a solid-state mechanism.[5] Cobalt centers in the structure are separated by 7.13 Å, and adjacent complexes are arranged in a C_2-symmetric fashion. The heterogeneous nature of the catalyst and inability to predict the solid-state packing of complexes made it difficult to improve catalyst performance by rational ligand modification, leading to the development of a discrete bimetallic complex mimicking the structural features seen in the unit cell of the crystal structure of **2**.

Received: September 13, 2013
Published: November 7, 2013

   dx.doi.org/10.1021/ja409521z | J. Am. Chem. Soc. 2013, 135, 18901−18911

Scheme 1. Isoselective and Enantioselective Polymerizations of Propylene Oxide Using Cobalt Catalysts

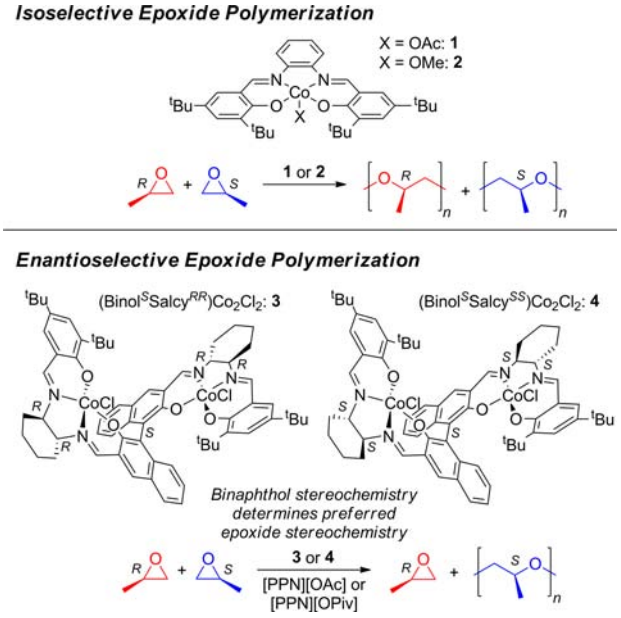

The bimetallic cobalt(III) complex, **3**, was prepared by attaching two salen moieties to a chiral binaphthol linker to achieve a favorable Co···Co separation for epoxide enchainment[5] and an almost perpendicular orientation of the salen planes. In the presence of bis(triphenylphosphine)iminium (PPN), phosphonium, or phosphazenium cocatalyst salts, such as PPN acetate ([PPN][OAc]) or PPN pivalate ([PPN][OPiv], pivalate = $^{t}BuCO_2^-$), **3** kinetically resolves racemic epoxides to yield highly isotactic polyethers and unreacted enantiopure epoxides.[6] The diastereomer of **3** synthesized using (1*S*,2*S*)-1,2-diaminocyclohexane and binaphthol with *S*-axial chirality, **4**, showed that the stereoselectivity of the catalyst is predominantly determined by the axial chirality of the binaphthol linker since complexes with *S*-axial chirality preferentially polymerize *S*-PO (and other terminal epoxides of the same relative configuration) with high selectivity factors (*s*-factor) that range from 50 to 300.[7]

Since **3** is the first well-defined catalyst that polymerizes a variety of racemic epoxides to form highly isotactic polyethers,[8] we initiated studies to elucidate the mechanism of this system. However, the paramagnetism of the catalyst, short reaction times resulting from high catalyst activity, and precipitation of semicrystalline polyether during polymerization made it extremely difficult to obtain reliable kinetic data or observe intermediates for traditional mechanistic studies. In this study, we propose a mechanistic hypothesis for the polymerization of monosubstituted epoxides by **3** on the basis of experimental observations and theoretical calculations. Considering the complex and multifaceted nature of the catalyst system, we investigated the mechanism of polyether synthesis by focusing on five key aspects: (1) the structural features of the catalyst, (2) the regio- and stereoselectivity of the chain-growth step, (3) the probable oxidation and electronic state of Co during the polymerization, (4) the role of the cocatalyst, and (5) the mechanism of monomer enchainment.

EXPERIMENTAL DETAILS

For information regarding experimental procedures, materials, and computational details, see the Supporting Information.

RESULTS AND DISCUSSION

Structural Features of the Catalyst. An X-ray crystal structure of the tetrapyridine adduct of **4**, **4**·py_4, was obtained and compared to the previously reported structure of **3**·py_4.[6b] In the solid state, **4**·py_4 had a more open cleft than **3**·py_4, with a Co···Co separation of 6.94 Å and an *endo* naphthyl−naphthyl

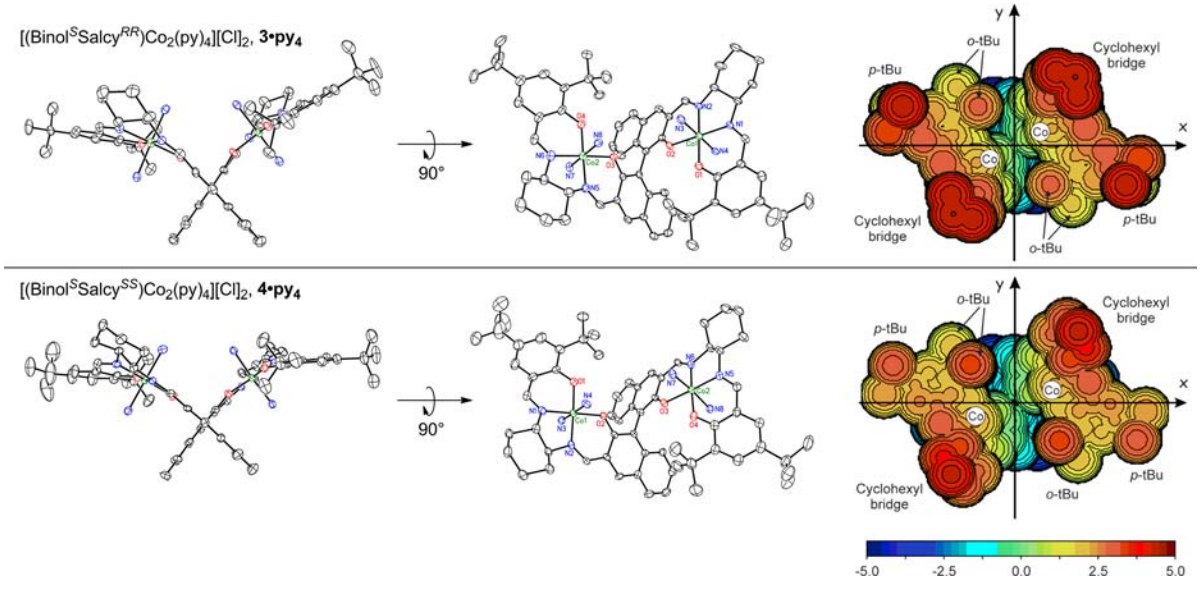

Figure 1. Comparison of the crystal structures of **3**·py_4[6b] and **4**·py_4. Thermal ellipsoids are shown at the 40% probability level, pyridine ligands are truncated, and hydrogen atoms and chloride ions are omitted for clarity. Also shown are topographic steric maps generated from the crystal structures, with chloride ions and pyridine ligands omitted. The midpoint of the Co atoms has been set at the origin, the C_2-symmetry axis has been oriented along the *z*-axis, and the binaphthol C−C bond has been set in the *yz* plane. The isocontour scale, in Å, is provided at the bottom of the figure. In the case of **3**·py_4, the crystal structure was obtained from a racemic mixture of **3**; the enantiomer of **3**·py_4 with *S*-binaphthol stereochemistry is shown.

dx.doi.org/10.1021/ja409521z | J. Am. Chem. Soc. 2013, 135, 18901−18911

dihedral angle of 90°, compared to 6.45 Å and 79°, respectively, for **3**·py_4. Topographic steric maps of **3**·py_4 and **4**·py_4, with pyridine molecules omitted for clarity, are shown in Figure 1 and provide a clear representation of the catalytic pocket in the two complexes.[9]

For both **3**·py_4 and **4**·py_4, the salen moieties shape a deep groove terminating with the binaphthol bridge. The Co atoms facing each other are anchored on opposite walls of the groove. Steric hindrance around the Co centers is provided by the cyclohexyl bridges and the *ortho*-^{t}Bu groups of the salicyl moieties. Consistent with the larger Co···Co separation for **4**·py_4, the cleft is more open, and the cyclohexyl bridges are slightly folded away from the central groove. The *para*-^{t}Bu groups of the salicyl moieties for both **3**·py_4 and **4**·py_4 are pointing away from the reactive pocket, and thus their effect on stereo- and regioselectivty can only be electronic in nature, though they may provide steric protection for the reactive metal centers, thereby improving stability and consequently activity.

In order to better understand the effect of the face-to-face orientation of the two salen planes, we calculated the percent buried volume[10] (%V_{Bur}), a measurement of the volume of a sphere of 3.5 Å around a metal center occupied by a ligand for **3**·py_4 and **4**·py_4. We initially used a single salen unit in order to estimate the %V_{Bur} around a Co center without influence of the other salen unit, with *endo* pyridines removed to mimic metal centers with a vacant coordination position ready to host an incoming epoxide molecule. This resulted in the rather high %V_{Bur} of 80.0% and 78.7% for the single salen units of **3**·py_4 and **4**·py_4, respectively. To estimate the steric impact of the second salen unit, we then calculated the %V_{Bur} around the same Co center using the full bimetallic structures of **3**·py_4 and **4**·py_4 with both *endo* pyridines removed, which resulted in %V_{Bur} values of 80.4% and 79.0% for **3**·py_4 and **4**·py_4, respectively. The negligible increase in the %V_{Bur} of the Co centers using a single salen unit or the full complex suggests that the binaphthol bridge provides an optimal placement of the two salen units without hindering accessibility to the Co centers.

Regio- and Stereoselectivity of the Chain-Growth Step. To gain insight into the origin of the regio- and stereoselectivity of epoxide enchainment, we relied on density functional theory (DFT) calculations. The model catalyst used in the DFT calculations, **5** (Figure 2), was similar to **3**, but for increased computational efficiency, a biphenol linker restricted to the *S* conformation was substituted for the *S*-binaphthol linker, and the *para*-salicyl substituent was removed. In the model, a PO molecule was coordinated to one of the Co centers inside the catalytic cleft of **5** and ring-opened by a methoxide (OMe) nucleophile coordinated to the adjacent Co (Figure 3). The chloride ions of the catalyst were placed in the *exo* positions, consistent with the need for cocatalyst salts to achieve polymerization activity in solution.[6a] The four transition states (TSs) shown in Figure 3 display the different possibilities for nucleophilic attack at the methylene (1,2-addition) or methine carbon (2,1-addition) of both PO enantiomers. Calculations showed that the favored TS corresponded to 1,2-addition of an *S*-PO molecule (**TS-1,2-*S***; Figure 3a). This agreed with experimental findings using **3**, where *S*-PO is preferentially enchained with retention of stereochemistry at the stereogenic methine carbon.[6a] The TS corresponding to the 1,2-addition of *R*-PO (**TS-1,2-*R***; Figure 3b) was 4.4 kcal/mol higher in energy relative to **TS-1,2-*S***, in agreement with the high stereoselectivity of the catalyst. The energy difference between **TS-1,2-*R*** and the favored **TS-1,2-*S*** is represented by the term $\Delta\Delta G_{Stereo}$ (*vide infra*). The two TSs corresponding to 2,1-addition of *S*- or *R*-PO (**TS-2,1-*S*** and **TS-2,1-*R***; Figure 3c,d) were respectively 3.5 and 4.8 kcal/mol higher in energy than the favored **TS-1,2-*S***, which was in agreement with the high regioselectivity experimentally observed for the **3**/[PPN][OAc] catalyst system.[6a] The energy difference between the lowest energy TS for 2,1-addition (**TS-2,1-*S***) and the favored **TS-1,2-*S*** is represented by the term $\Delta\Delta G_{Regio}$ (*vide infra*).

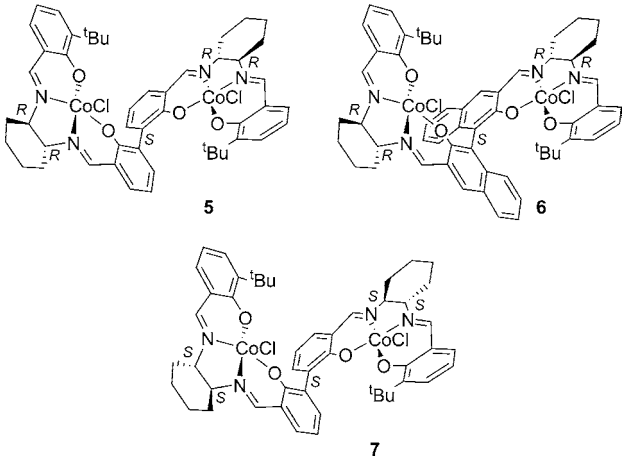

Figure 2. Bimetallic complexes used for calculations.

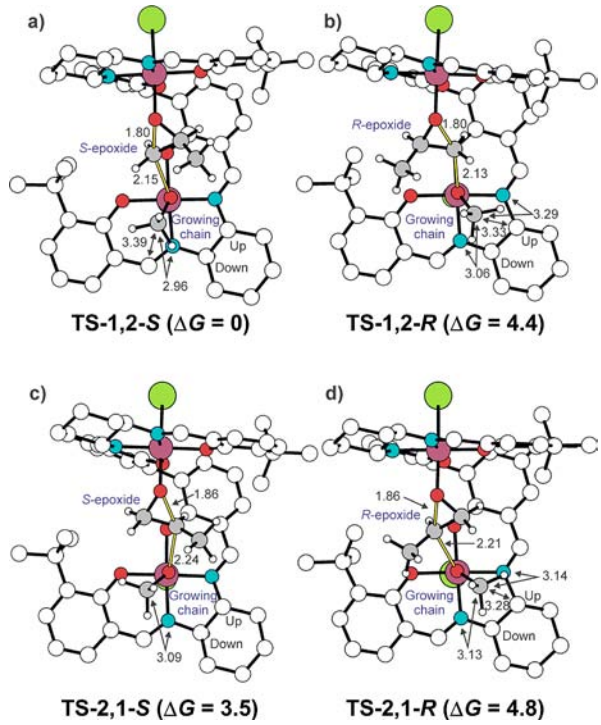

Figure 3. Four possible transition states for the ring-opening of a PO molecule by an adjacent cobalt-bound methoxide group, based on **5** with *exo* chlorides: (a) **TS-1,2-*S***, ring-opening of *S*-PO at the methylene carbon; (b) **TS-1,2-*R***, ring-opening of *R*-PO at the methylene carbon; (c) **TS-2,1-*S***, ring-opening of *S*-PO at the methine carbon; (d) **TS-2,1-*R***, ring-opening of *R*-PO at the methine carbon. Distances in Å, free energies in kcal/mol.

dx.doi.org/10.1021/ja409521z | J. Am. Chem. Soc. 2013, 135, 18901−18911

In order to validate the use of **5** as a computational model, calculations were also conducted using **6**, which is identical to **3** except for the substitution of the *para*-^{t}Bu groups for H, with a OMe nucleophile and revealed that $\Delta\Delta G_{Stereo}$ = 4.2 kcal/mol with **TS-1,2-*S*** favored, while $\Delta\Delta G_{Regio}$ = 4.1 kcal/mol with **TS-2,1-*S*** lower in energy than **TS-2,1-*R***. The most favorable transition state, **TS-1,2-*S***, presented a naphthyl−naphthyl dihedral angle of 75.8° and a Co···Co separation of 6.29 Å. These values are comparable to the corresponding parameters observed in the crystal structure of **3**·**py**$_4$.[6b] The $\Delta\Delta G_{Stereo}$ and $\Delta\Delta G_{Regio}$ values calculated using **6** are similar to those observed when using **5**, indicating that **5** is a viable computational model of **3**.

Calculations with **7**, a model compound for **4** with (1*S*,2*S*)-1,2-diaminocyclohexane and a biphenol linker restricted to the *S* conformation, with a OMe nucleophile resulted in a lower $\Delta\Delta G_{Stereo}$ = 3.1 kcal/mol and $\Delta\Delta G_{Regio}$ = 3.0 kcal/mol, with **TS-1,2-*S*** the favored transition state. This is in agreement with the lower selectivity factors observed for **4** compared to **3**.[7] Calculations predict that both **6** and **7** select for *S*-PO, matching the observed experimental results for **3** and **4**.

Although these calculations explained the remarkable stereoselectivity of the catalysts, they suggested that polymer regioerrors should occur more frequently than stereoerrors, since $\Delta\Delta G_{Stereo} < \Delta\Delta G_{Regio}$. Experimentally only polymer stereoerrors are observed. To resolve this discrepancy, we examined the ring-opening of PO using an isopropoxide (O^iPr) group to more accurately simulate the growing polymer chain with **5** as the model catalyst. The resulting values of $\Delta\Delta G_{Stereo}$ = 3.2 kcal/mol and $\Delta\Delta G_{Regio}$ = 4.6 kcal/mol are more representative of the polymer microstructure defects observed.

We next moved to rationalize the origin of regio- and stereoselectivity in these complexes by inspection of the TSs of **5** shown in Figure 3. No steric interactions were observed between the PO coordinated to one of the Co centers and the ligand framework, since the PO is mainly oriented in the mean plane bisecting the groove shaped by the two salen moieties. Rather, selectivity appeared to correspond to the orientation of the methyl group of the methoxide. In **TS-1,2-*R***, this methyl group was oriented toward the diaminocyclohexane bridge, whereas in **TS-1,2-*S***, it was oriented toward the flat and less bulky phenoxyimine. This resulted in a series of short distances between the methyl group and C atoms of the ligand for **TS-1,2-*R*** (see Figure 3b). The methyl group was similarly oriented in the regioirregular **TS-2,1-*S*** and **TS-2,1-*R*** transition states, and again the transition state with the methyl group closer to the diaminocyclohexyl bridge (**TS-2,1-*R***) was higher in energy. This finding is consistent with the works of Kemper et al.[11] and Jacobsen et al.[12] in which monometallic (salen)Co complexes used for highly stereoselective epoxide hydrolysis were found to bind epoxides with only a moderate degree of stereoselectivity. Instead, the main source of stereoselectivity was a bimetallic TS in which nucleophilic attack on the matched epoxide complex is sterically more favorable than on the mismatched epoxide complex. It is also similar to the isotactic polymerization of propene by *ansa*-metallocene catalysts, in which the ligand chirality dictates the chiral orientation of the growing polymer chain, which in turn stereoselectively selects among the two prochiral faces of propene for insertion into the alkyl chain.[13]

The influence of the dihedral angle, ϕ, of the biaryl bridge on stereoselectivity was then investigated by calculating $\Delta\Delta G_{Stereo}$ as a function of the angle ϕ of **5**. Figure 4a clearly shows that both the **TS-1,2-*S*** and **TS-1,2-*R*** curves followed a similar

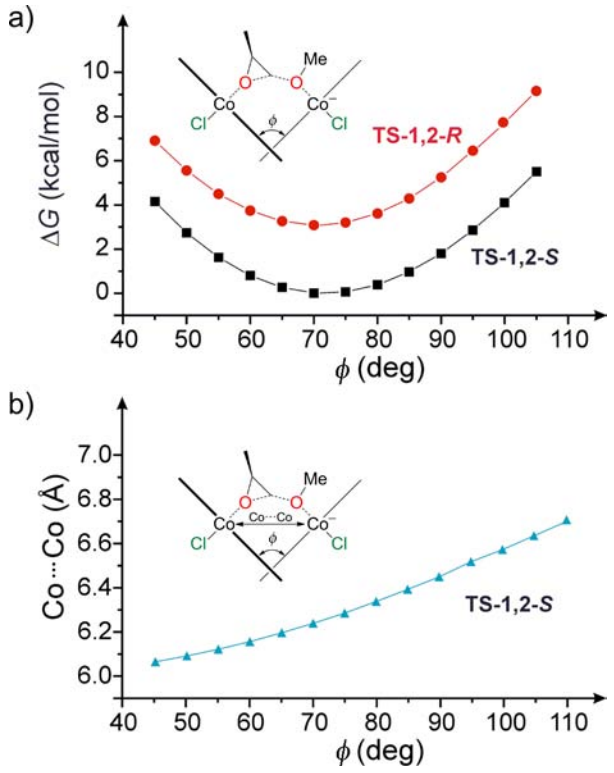

Figure 4. Effect of varying the dihedral angle ϕ of an active catalyst based on **5** on (a) the energy of the **TS-1,2-*S*** and **TS-1,2-*R*** transition states with respect to the minimum ΔG of **TS-1,2-*S*** and (b) the Co···Co separation of the favored **TS-1,2-*S***.

trend, implying that the $\Delta\Delta G_{Stereo}$ was insensitive to this parameter and that the stereoselectivity was barely influenced by fluctuations of the complex. The optimal value for ϕ was around 70°, and could vary between 60° and 80° with a ΔG penalty of <1 kcal/mol, indicating a reasonable degree of flexibility in the complex. Despite this flexibility, the variation of the Co···Co separation in **TS-1,2-*S*** was roughly limited in the 6.1−6.3 Å range for values of ϕ between 60° and 80° (Figure 4b). The flexibility of the ligand framework, coupled with a relatively stable Co···Co separation, is potentially relevant for the catalytic functionality.

To further probe the relationship between the stereochemistries of the biaryl bridge and the chiral diamine linker with respect to the stereochemistry of epoxide enchainment, we synthesized **8** (Figures 5 and 6), with the same diamine stereochemistry as **3** but an achiral biphenol linker instead of the *S*-binaphthol linker. The crystal structure of **8**·**py**$_4$ (Figure 5) showed that it was present in only one of its two possible pseudo-diastereomers, with the achiral biphenol bond in the same relative orientation as *S*-binaphthol. The Co···Co separation of 6.59 Å and *endo* phenyl−phenyl dihedral angle of 79° were similar to the corresponding values for **3** and **4**. Complex **8** was also active for the polymerization of PO when combined with [PPN][OPiv], showing lower activity (turnover frequency = 490 h^{-1}) and stereoselectivity (selectivity factor = 32) compared to **3** and **4**. Chiral gas chromatography of the unreacted epoxide revealed that **8** selectively polymerized *S*-PO, matching the experimental results when using **3** and the computational studies of this work. In addition, the stereodefects of the polymer were consistent with an enantiomorphic site control mechanism. While the above evidence suggests that

dx.doi.org/10.1021/ja409521z | J. Am. Chem. Soc. 2013, 135, 18901−18911

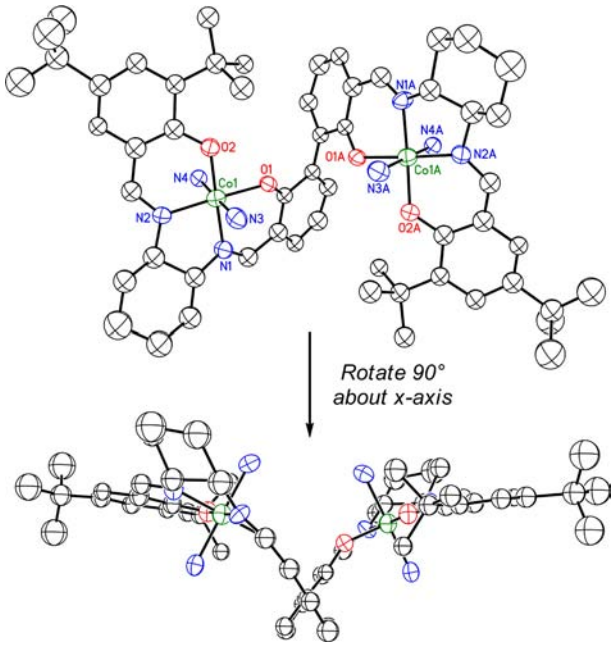

Figure 5. Crystal structure of complex **8**·py_4, with hydrogen atoms and chloride ions omitted and pyridine ligands truncated for clarity. The Co, N, O, and Cl atoms were refined anisotropically, and the C atoms were refined isotropically. Thermal ellipsoids are shown at the 30% probability level.

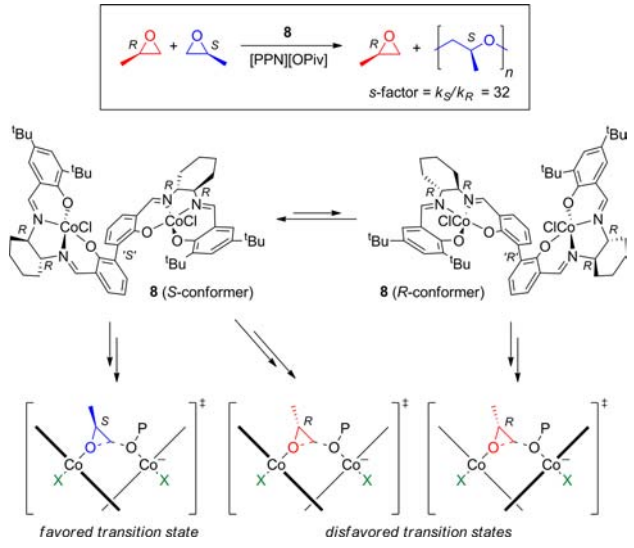

Figure 6. Enantioselective polymerization of PO using **8**, with possible conformers and transition states.

the *S*-conformer of **8** and the associated TS are energetically favored over the *R*-conformer and TS, we are unable to determine at this time if the lower stereoselectivity of **8** is due to a less selective *S*-conformer TS that allows incorporation of *R*-PO or if the stereoerrors originate from a small amount of the *R*-conformer that may be present under polymerization conditions (Figure 6).

Oxidation and Electronic State of Co in the Catalyst. In order to elucidate the mechanism of epoxide enchainment, we considered the possible oxidation states of the cobalt centers during polymerization. The crystal structures of **3**·py_4[6b] and **4**·py_4[7] display two pyridine molecules coordinated to each Co and a respective chloride anion in close proximity to the metal centers. Complexes **3** and **4** are also diamagnetic in pyridine-d_5 yet paramagnetic in nondonating solvents, consistent with bimetallic Co(III)−Co(III) complexes where both Co centers are low-spin in a donating solvent. Although these data suggest that the cobalt centers of the active catalyst are in +3 oxidation states, they alone do not eliminate the possibility of having Co(II)−Co(II) or Co(II)−Co(III) species generated by full or partial reduction of the starting Co(III)−Co(III) precatalyst.

The Co(II)−Co(II) precursor to **3** was inactive for the polymerization of PO under all reaction conditions tested. We propose that a PO molecule can coordinate to the Co(II) centers, but the absence of an eligible nucleophile on an adjacent metal center eliminates the possibility for initiation. Therefore, it is unlikely that a Co(II)−Co(II) complex is involved in the polymerization.

The possibility of a Co(II)−Co(III) species catalyzing the polymerization was also explored. This mechanism requires generation of a Co radical and enchainment of epoxide through a radical mechanism.[14] However, when rigorously pure and dry epoxide monomers and solvents were used, the polymerization began immediately upon addition of epoxide. This suggested that the active catalyst is the starting Co(III)−Co(III) species. Additionally, these polymerizations can be run under an oxidative atmosphere of dry air. Since the intermediacy of Co(II)−Co(II) and Co(II)−Co(III) oxidation states appears unlikely on the basis of the experimental findings, we propose that the catalyst exists as a Co(III)−Co(III) species throughout the reaction.

Having concluded that the active catalyst exists as a Co(III)−Co(III) species, we then investigated the electronic state of the system computationally. We evaluated the relative stability of the high-spin (triplet) and low-spin (singlet) electronic states for the model monometallic complex **9**, with the results shown in Table 1, and the model bimetallic complex **5**, with the results shown in Figure 7. Calculations indicated that the high-spin state was favored by 13.8 kcal/mol for the mono-ligated species **9a**. This was rationalized by the vacant coordination position of the Co center of **9a**, resulting in reduced field splitting. In the presence of a weak-field PO molecule, it was not possible to optimize the geometry with the PO molecule coordinated to a high-spin Co center, as the PO molecule was repelled. The best geometry found was an adduct with the PO molecule at 2.75 Å from the metal. Conversely, clear coordination was achieved in

Table 1. DFT Calculated Free Energy of the High-Spin (Triplet) Electronic State Relative to the Low-Spin (Singlet) Electronic State, in kcal/mol, for Various Ligands Bound to 9[a]

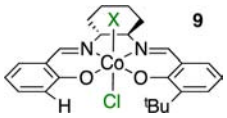

		$\Delta G_{HS} - \Delta G_{LS}$	
X	complex	M06	M06L
–	**9a**	−13.8	−4.6
Cl	**9b**	0.8	9.0
OAc	**9c**	0.5	6.8
OMe	**9d**	4.2	14.6

[a]Complexes **9b**−**d** have a formal negative charge on the complex. The M06 and M06L values were obtained using the M06 and M06L functional in the single-point energy calculation in solution.

dx.doi.org/10.1021/ja409521z | J. Am. Chem. Soc. 2013, 135, 18901−18911

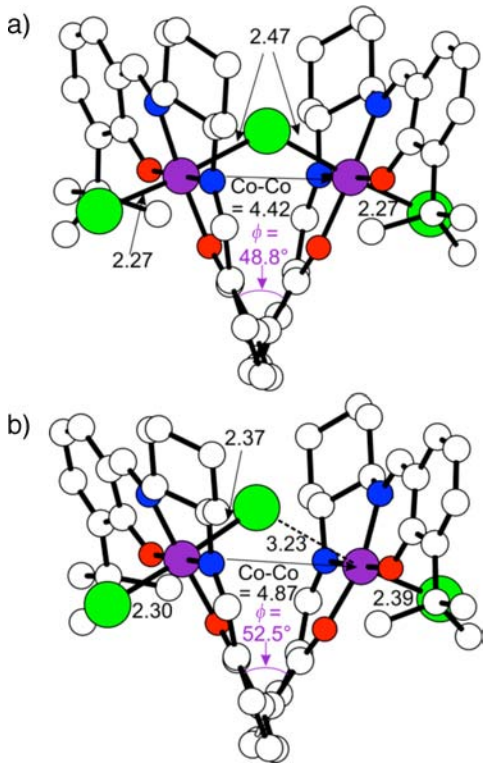

Figure 7. DFT optimized geometries of complex **5** with an additional chloride ligand: (a) both Co centers low-spin and (b) a mixed-spin-state complex, with a bis-ligated low-spin Co center and a mono-ligated high-spin Co center. Distances in Å.

the low-spin state with the PO at 2.10 Å from the metal. This indicated that PO coordination was favorable in the low-spin state but unfavorable in the high-spin state. The presence of a chloride or acetate ligand in the empty coordination site of **9a**, as in species **9b** and **9c**, resembles the situation at a Co center in the initiation step and resulted in a small preference for the low-spin state. For species **9d**, the hard methoxy ligand, which simulates the alkoxide chain end, caused the low-spin state to be preferred by 4.2 kcal/mol.

Overall, the results reported in Table 1 are consistent with the experimental evidence that in pyridine **3** and **4** are diamagnetic, while in nondonating solvent they are paramagnetic. Despite the consistency between experiments and theory, note that the exact quantification of energy difference between the high-spin and the low-spin states is quite sensitive to the specific density functional and is still a challenge for DFT. Usually, hybrid functionals are biased in favor of the high-spin state, while nonhybrid functionals are biased in favor of the low-spin state.[15] For this reason, we calculated the relative stability of the same species using the M06L functional, which has no Hartree–Fock exchange term and is biased toward a higher stability of the low-spin state.[16] The M06L results reported in Table 1 confirm the scenario provided by the M06 functional, with the high-spin state favored for **9a**, although the preference over the low-spin state is reduced from 13.8 to 4.6 kcal/mol, while the low-spin state is clearly favored for **9b–d**. The overall consistency between experimental evidence and the M06 and M06L results supports our conclusion about the preference for the high-spin state in the case of pentacoordinate Co centers and a preference for the low-spin state in the case of hexacoordinate Co centers. A recent study by Jacobsen et al. also found that the metal centers in pentacoordinated (salen)Co(OH) complexes are high-spin, while the metal centers of hexacoordinated (salen)Co(OH)(H_2O) complexes are low-spin.[12]

Having established the electronic state of monometallic complexes, we then investigated the electronic state of bimetallic complexes with three anionic ligands using **5** as a model. We found that a mixed-spin state (with a total spin density corresponding to two unpaired electrons) was favored, being 7.2 kcal/mol lower in energy than the low-spin state. This value is reduced to 1.0 kcal/mol only by the M06L functional, with no Hartree–Fock term.[16] The different stability of the low-spin state versus the mixed-spin state was a consequence of the symmetric binding of the *endo* chloride to both Co atoms, disfavoring the low-spin state on both metal centers shown in Figure 7a. In the mixed-spin state shown in Figure 7b, the *endo* chloride was clearly bound to only one Co atom, favoring an overall low-spin state on the bis-ligated Co center, while the other Co was 3.23 Å away from the *endo* chloride and in a high-spin state as a mono-ligated Co center. This binding scheme was achieved with a minimal variation in the ϕ angle, although the Co···Co separation was roughly 0.4 Å longer.

Role of the Cocatalyst. Cocatalysts have historically played an important role in the polymerization and copolymerization of epoxides by enhancing catalyst activity and enabling milder reaction conditions.[17] Bis(triphenylphosphine)iminium (PPN) salts, which contain a non-coordinating and unreactive cation and a strong axial σ donor anion, are particularly useful for cobalt-mediated copolymerizations of epoxides and carbon dioxide.[17g,h] Complex **3** and related compounds are active for the polymerization of epoxides in solution when combined with a PPN salt,[6a] but inactive in the absence of a cocatalyst. Initial results showed that acetate is an effective counteranion, giving molecular weight distributions of ∼2 and high turnover frequencies. Later work established that [PPN][OPiv] increases activity and selectivity of some of the related catalyst systems.[7] We postulate that only one anion per catalyst system can initiate a polymer chain in the absence of chain-transfer agents, as *exo* ligands are incapable of initiation due to their location *trans* to the active site. However, we cannot rule out a mechanism in which anion exchange gives *exo* ligand polymer

Table 2. Effect of Varying the Catalyst-to-Cocatalyst Ratio Using 3 for PO Polymerization[a]

entry	3:[PPN][OPiv]	conv[b] (%)	*mm*[c] (%)	$ee_{polymer}$[d] (%)	M_n[e]	M_w/M_n[e]	*s*-factor[f]
1	1:1	10	99.1	99.4	43.6	3.5	>300
2	1:2	25	98.8	99.1	126	2.3	>300
3	1:4	30	98.6	99.1	106	2.4	>300

[a]Polymerization conditions: [PO] = 1 M in DME; [PO]:[**3**] = 20,000:1; t_{rxn} = 10 min; T_{rxn} = 0 °C. [b]Determined gravimetrically. [c]Determined by ^{13}C NMR spectroscopy. [d]Calculated using $ee_{(polymer)} = (2[mm] + [mr] + [rm] - 1)^{1/2}$.[6a] [e]Determined by gel-permeation chromatography in tetrahydrofuran at 30 °C calibrated with polystyrene standards. [f]Calculated using *s*-factor = $\ln[1 - c(1 + ee_{(polymer)})]/\ln[1 - c(1 - ee_{(polymer)})]$.[6a]

dx.doi.org/10.1021/ja409521z | J. Am. Chem. Soc. 2013, 135, 18901–18911

alkoxides and *endo* chloride or acetate ions, which could initiate new polymer chains.

We next investigated the influence of the cocatalyst on the polymerization by varying the catalyst-to-cocatalyst ratio used in the polymerization system. We used the more active cocatalyst [PPN][OPiv] with **3** for this study. As can be seen in Table 2, the change in catalyst-to-cocatalyst ratio did not have an appreciable effect on the stereoselectivity of the catalyst, as evidenced by the isotacticity of the polymer product. Polymerizations with >1 equiv of cocatalyst achieved higher turnover frequencies. Increasing the number of cocatalyst equivalents relative to catalyst to 4 from 2 led to the lowering of the M_n of the polymer produced, even as the theoretical M_n of the polymer was increased due to the higher percent conversion of epoxide to polyether. This may be due to chain transfer between the polymer chains and excess cocatalyst, leading to an increase in the number of chain initiators present in the system.

To further understand the role of anion binding and exchange with these catalysts, we performed DFT calculations on the binding free energy of chloride and acetate anions to the monometallic (salen)CoX unit of model compound **9** (Figure 8), which lacks *para*-^{t}Bu groups to save computational time.

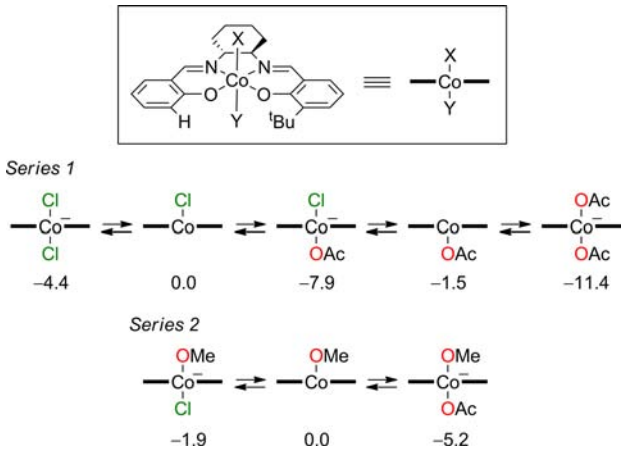

Figure 8. DFT calculated free energies, in kcal/mol, of monometallic (salen)Co complexes with bound chloride, acetate, and methoxide anions. The most stable electronic states of the mono- and bis-coordinated species are the triplet and singlet states, respectively.

Calculations showed that $[(salen)CoX_2]^-$ species were more stable than (salen)CoX species. In accordance with the results shown in Table 1, coordination of a second anion also changed the electronic state of the cobalt center from the triplet state, which was the most stable state in the mono-coordinated species, to the singlet state in the bis-coordinated species. Comparison between the respective mono-ligated species indicated that the mono-ligated (salen)CoOAc species was only 1.5 kcal/mol lower in energy than the mono-ligated (salen)CoCl species. As these differences were close to the margin of error for these calculations, we could only conclude that binding of the two anions to a Co center is competitive, although coordination of acetate was slightly favored over chloride. The energy profile of Figure 8, Series 1 also provides a possible mechanism for anion exchange between a (salen)CoX species and [PPN][OAc]. Figure 8, Series 2 shows the binding energy of the anion in the presence of an alkoxide ligand, simulating the growing polyether chain. Coordination of the anion trans to the hard alkoxide ligand was less favored relative to coordination trans to a softer ligand such as acetate. For example, dissociation of chloride from the MeO−Co−Cl bis-ligated species cost only 1.9 kcal/mol, compared to the 6.4 kcal/mol required to dissociate Cl from the AcO−Co−Cl bis-ligated species. The rather weak binding energy of the compounds in Figure 8, Series 2 suggested that the anion could even dissociate during polymerization.

Next we examined anion binding and exchange with the model bimetallic complex **5** as shown in Figure 9. The net

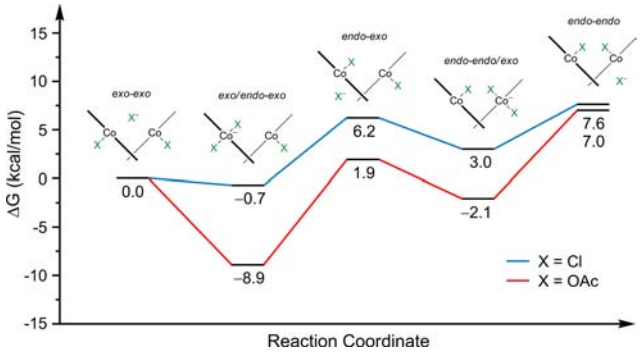

Figure 9. Interconversion of diastereomers of **5** in the presence of chloride and acetate ions.

result of anion coordination and de-coordination for the bimetallic complex is interconversion between *exo-exo* and *endo-endo* isomers. Consistent with the results shown in Table 1 and Figure 7, mono- and bis-ligated Co centers are calculated as high- and low-spin, respectively. For species with only mono-ligated Co centers, for chloride and acetate ligands the *endo-exo* isomer was 6.2 and 1.9 kcal/mol less stable, respectively, than the *exo-exo* isomer, while the *endo-endo* isomer was 7.6 and 7.0 kcal/mol less stable, respectively, than the *exo-exo* isomer. The lower stability of the *endo-endo* isomer can be easily related to repulsive interactions between the two adjacent anions. Connection between the various mono-ligated diastereomers was provided by species presenting one bis-ligated Co center and one mono-ligated Co center. The *exo/endo-exo* species was more stable than the *exo-exo* isomer by 0.7 and 8.9 kcal/mol for chloride and acetate ligands, respectively. The *endo-endo/exo* species was disfavored by 3.0 kcal/mol for chloride ligands and favored by only 2.1 kcal/mol for acetate ligands relative to the *exo-exo* species, the reduced stability a consequence of a repulsive interaction between the two *endo*-coordinated ligands. Overall, these results suggested that the dominating species in solution should correspond to a system presenting a bis-ligated Co and a mono-ligated Co with a vacant *endo* coordination site. Coordination of a free PO molecule to this vacant *endo* coordination site occurs prior to initiation.

We then modeled the ring-opening of PO using a chloride or pivalate nucleophile bound to **5**, a situation that resembles the initiation of polymerization when using cocatalyst [PPN][OPiv] (Figure 10). The energy profile shown in Figure 9 suggests that multiple species are likely present in the reaction system, requiring simplification of the computational system to the *exo-exo* bis-chloride species as the reference structure in order to ensure computational feasibility. The first step was coordination of the pivalate anion, leading to the anion adduct (AA), which changed the spin state of the coordinated Co center from high- to low-spin. The two isomers that could be formed by pivalate anion coordination were similar in energy,

dx.doi.org/10.1021/ja409521z | J. Am. Chem. Soc. 2013, 135, 18901−18911

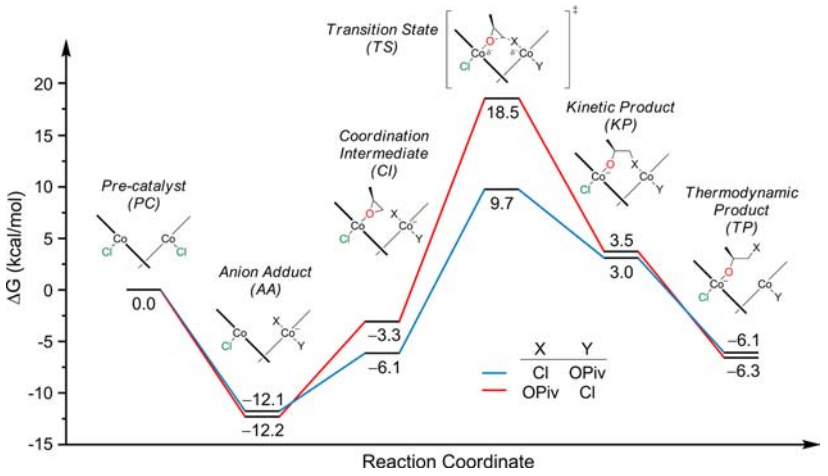

Figure 10. DFT calculated free energies of initiation steps using **5**. Mono- and bis-coordinated Co centers are calculated as high- and low-spin, respectively.

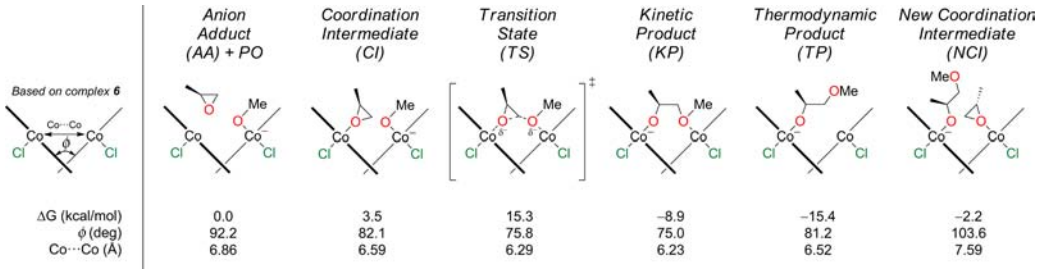

Figure 11. DFT calculated free energies, dihedral angles, and Co···Co separations for propagation steps based on **3**. Mono- and bis-coordinated Co centers are calculated as high- and low-spin, respectively.

roughly 12 kcal/mol more stable than the starting *exo-exo* bis-chloride species (the isomer with the pivalate anion in the *exo* position could be formed through a sequence of steps similar to those presented in Figure 9). Coordination of PO to the adjacent Co center, which required a change of the spin state of that Co center from high- to low-spin, was endergonic and led to the coordination intermediate (CI). The isomer with the pivalate anion in the *endo* position, at −3.3 kcal/mol, was slightly higher in energy than the isomer with the pivalate anion in the *exo* position, at −6.1 kcal/mol, due to repulsive interactions between the bulky pivalate anion and the PO. The TS for ring-opening of epoxide by the chloride anion was lower in energy compared to that for ring-opening by the bulkier pivalate anion, as can be seen when comparing the TSs in Figure 10. The TS involving the pivalate anion was disfavored mainly due to the breaking of the strong Co−OPiv bond, though steric repulsion due to the larger pivalate anion also contributed. After ring-opening, the system collapsed to the kinetic product (KP), where the chloride or pivalate chain end remained associated with the Co center to which it was originally coordinated in the CI step. Dissociation of these groups was energetically favored, and was driven by a change of the spin state of the corresponding Co center from low- to high-spin, leading to the thermodynamic product (TP). Similar to the case of olefin epoxidation by (salen)Mn catalysts,[15b,18] it is impossible to indicate if this change in the spin state from low to high actually occurs, as it is possible that a new PO molecule displaces the coordinated chloride or pivalate chain ends, preventing spin-crossing to the high-spin state and allowing the full reaction pathway to occur in the low-spin state. This consideration also holds for the chain-growth step discussed in the next section.

Mechanism of Chain-Growth. After establishing a hypothesis for the role of the cocatalyst for initiation, we began to model the mechanism of propagation. Calculations were performed using **6**, with two *exo*-chloride anions and an *endo*-methoxide anion to represent the propagating polyether chain (Figure 11). As in initiation, the first step was coordination of a PO molecule to the Co center with a free *endo* coordination site to form the CI, followed by a TS in which the epoxide was ring-opened via nucleophilic attack at the methylene carbon by the methoxide anion. After epoxide ring-opening, the KP had the oxygen of the terminal methoxy group associated with the Co center to which it was coordinated in the CI step. The oxygen of the terminal methoxy chain end could then dissociate as a consequence of a change in the spin state of the coordinated Co atom from low-spin to high-spin, leading to the most stable TP species, or be displaced by another epoxide molecule, leading to a new coordination intermediate (NCI). The calculated ΔG values indicate that formation of the CI and the TS was relatively endergonic, but the system collapsed to a rather stable species after ring-opening of the epoxide. Coordination of a new PO molecule was again endergonic, but the overall free energy change from the first CI to the second CI was negative.

We also calculated the geometrical effects that PO enchainment has on the bimetallic complex. Figure 11 shows the value assumed by the dihedral angle ϕ and the Co···Co separation during PO enchainment. The CI had the largest ϕ angle and largest Co···Co separation of the steps to incorporate the first epoxide in order to accommodate both the epoxide and the

dx.doi.org/10.1021/ja409521z | J. Am. Chem. Soc. 2013, 135, 18901−18911

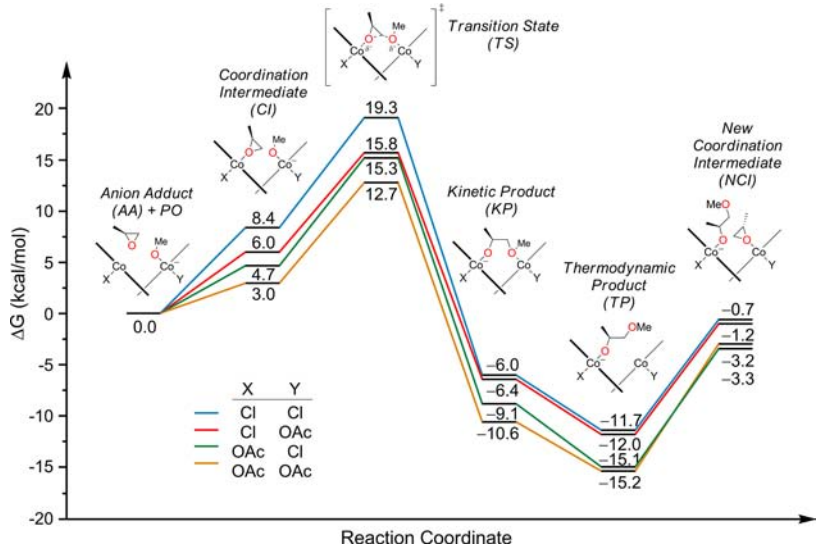

Figure 12. DFT calculated free energy diagram of PO enchainment using a methoxide propagating group and **5** with different *exo* axial ligands.

Scheme 2. Proposed Catalytic Cycle for the Polymerization of PO with Precatalyst 3 and a Cocatalyst Salt

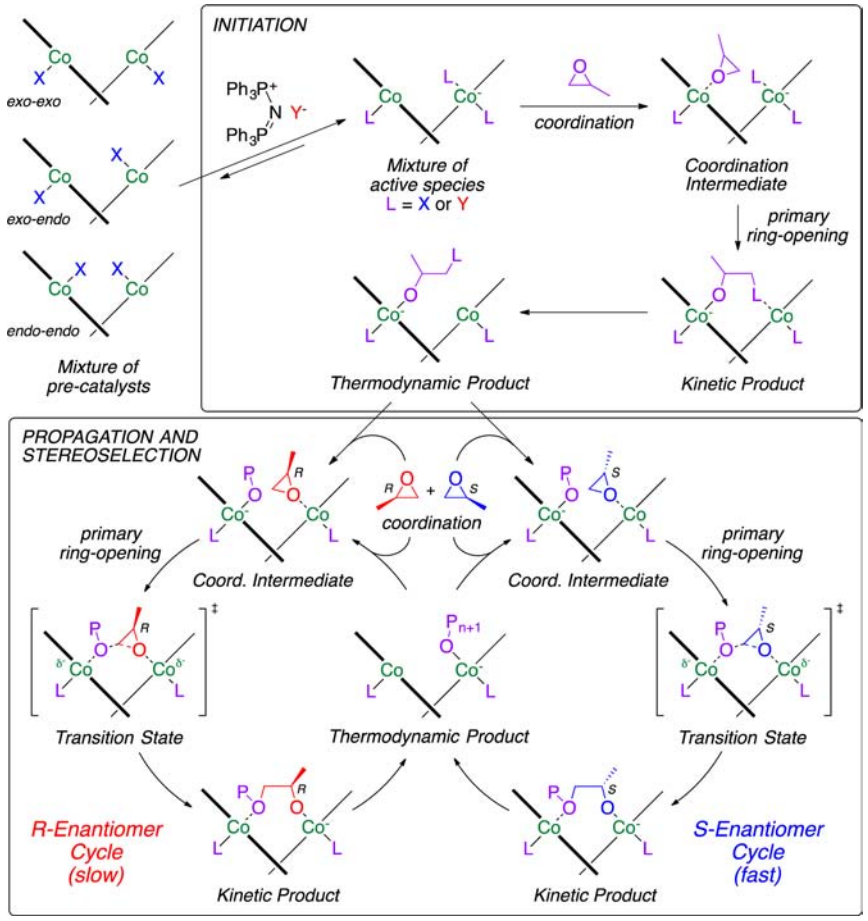

methoxide in the catalyst cleft. As expected, the TS displayed smaller values for both geometrical parameters than the CI, while the KP had the smallest values for both geometrical parameters due to the coordination of the terminal methoxy oxygen atom to the adjacent Co center. The NCI required a ϕ nearly 30° larger and a Co···Co separation over 1.3 Å longer than observed in the KP. These data are consistent with the plots of Figure 4, confirming that flexibility around the dihedral angle ϕ is fundamental for catalytic functionality, as it allows variations of the Co···Co separation in order to satisfy the geometric requirements of monomer enchainment.

The nature of the axial ligand of (salen)Co(III) complexes has a strong influence on the rate of epoxide hydrolysis.[19] Therefore, the effects of the axial ligands on the enchainment of a PO molecule were investigated. To save computational time, the model complex **5** was used with *exo* chloride and acetate

dx.doi.org/10.1021/ja409521z | J. Am. Chem. Soc. 2013, 135, 18901−18911

anions as axial ligands, and the calculated energy profiles are reported in Figure 12. Calculations indicate that all combinations of *exo* chloride and acetate ligands resulted in thermodynamically favorable enchainment pathways, since all the PO addition products are clearly lower in energy than the starting species. Differences between the various pathways are small, although it is quite clear that the most energetically favorable pathway for propagation was observed when both *exo* ligands are acetates (orange line in Figure 12).

CONCLUSION

In conclusion, we were able to combine experimental observations and theoretical calculations to examine (a) the origin of stereoselectivity in the catalyst cleft, (b) the importance of a flexible Co···Co separation, (c) the electronic state of the Co(III) metal centers during the polymerization, (d) the ability of the cocatalyst to interconvert the *exo-exo*, *exo-endo*, and *endo-endo* forms of the catalyst and its role in initiation and propagation, and (e) the free-energy profile of epoxide enchainment. Scheme 2 shows our proposed comprehensive mechanism for epoxide enchainment.

The mechanism we propose is reminiscent of the elegant work done by Okuda et al., who demonstrated that a 1:1 mixture of an aluminum complex and an aluminate complex was active for the regioselective polymerization of PO. They proposed that the transition state for epoxide enchainment in their system is bimetallic, encompassing a Lewis acidic aluminum complex activating PO, while a nucleophilic alkoxide from an aluminate complex ring opens the epoxide.[20]

Our mechanism is conceptually similar, but by linking the two metal centers in close proximity, the barrier to a bimetallic TS is minimized, and the geometry of the complex is able to dictate the regio- and stereoselectivity of the polymerization. As shown in Figure 10, the barrier to initiation was minimized when a chloride ion ring opens PO, while Figure 12 shows that, for the sequential enchainment of PO, acetate ligands were preferred as *exo* ligands.

We plan to use the information gained by this study to design new bimetallic catalysts that are active for the polymerization of more substituted epoxides, give polymers with narrower molecular weight distributions, and are simpler to synthesize. Changing the sterics and electronics of the catalysts, the use of tethered cocatalysts, and new bimetallic ligand architectures are currently being explored in our laboratory.

ASSOCIATED CONTENT

Supporting Information

Coordinate data sets and absolute energies for DFT optimized complexes, computational details, polymer characterization, calculation of $ee_{polymer}$ values and selectivity factors, full synthesis and characterization of **8**, polymerization procedures, and single-crystal X-ray diffraction data. This material is available free of charge via the Internet at http://pubs.acs.org.

AUTHOR INFORMATION

Corresponding Authors

coates@cornell.edu
luigi.cavallo@kaust.edu.sa

Notes

The authors declare no competing financial interest.

ACKNOWLEDGMENTS

We thank the NSF (CHE-1136607 and CHE-1112278) and the King Abdullah University of Science and Technology (KAUST; Award KUS-C1-018-02) for financial support. We also thank Dr. Ivan Keresztes and Mr. Anthony Condo for assistance with NMR experiments to confirm the structure of **8**. A.P. thanks the Spanish MINECO for a Ramón y Cajal contract (RYC-2009-5226), European Commission for a Career Integration Grant (CIG09-GA-2011-293900), and Generalitat de Catalunya (2012BE100824).

REFERENCES

(1) For a review, see: Ajiro, H.; Widger, P. C. B.; Ahmed, S. M.; Allen, S. D.; Coates, G. W. Stereoselective Ring-Opening of Epoxides. In *Polymer Science: A Comprehensive Reference*; Matyjaszewski, K., Möller, M., Eds.; Elsevier: Amsterdam, 2012; pp 165−181.

(2) Takeda and Inoue developed an aluminum porphyrin complex that produces PPO with an *mm*-triad content of 45% and a TOF of 400 h^{-1}. Borgne et al. showed that the stereoselectivity is due to a chain-end control mechanism (a) Takeda, N.; Inoue, S. *Makromol. Chem.* **1978**, *179*, 1377−1381. (b) Borgne, A. L.; Spassky, N.; Jun, C. L.; Momtaz, A. *Makromol. Chem.* **1988**, *189*, 637−650. Tsurata et al. developed a zinc alkoxide cluster (characterized by X-ray crystallography) that gives PPO with a *m*-dyad content of 79% and a TOF of 0.9 h^{-1}. (c) Yoshino, N.; Suzuki, C.; Kobayashi, H.; Tsuruta, T. *Makromol. Chem.* **1988**, *189*, 1903−1913. (d) Hasebe, Y.; Tsuruta, T. *Makromol. Chem.* **1988**, *189*, 1915−1926. Spassky et al. developed an aluminum salen complex that oligomerizes PO with an *s*-factor of 1.3 and a TOF of 0.2 h^{-1}. (e) Vincens, V.; Borgne, A. L.; Spassky, N. *Makromol. Chem. Rapid Commun.* **1989**, *10*, 623−628.

(3) (a) Pruitt, M. E.; Baggett, J. M. (Dow Chemical Co.). Catalysts for the Polymerization of Olefin Oxides. U.S. Patent 2,706,181, 1955. (b) Pruitt, M. E.; Baggett, J. M.; Bloomfield, R. J.; Templeton, J. H. (Dow Chemical Co.). Polymerization of Olefin Oxides. U.S. Patent 2,706,182, 1955. (c) Pruitt, M. E.; Baggett, J. M. (Dow Chemical Co.). Solid Polymers of Propylene Oxide. U.S. Patent 2,706,189, 1955. (d) Price, C. C.; Osgan, M.; Hughes, R. E.; Shambelan, C. *J. Am. Chem. Soc.* **1956**, *78*, 690−691. (e) Price, C. C.; Osgan, M. *J. Am. Chem. Soc.* **1956**, *78*, 4787−4792. (f) Vandenberg, E. J. *J. Polym. Sci.* **1960**, *47*, 486−489. (g) Vandenberg, E. J. (Hercules Powder Co.). Organoaluminum Oxide Catalyst Composition. U.S. Patent 3,219,591, 1965. (h) Vandenberg, E. J. *J. Polym. Sci., Part A: Polym. Chem.* **1969**, *7*, 525−567. (i) Vandenberg, E. J. *J. Polym. Sci., Part A: Polym. Chem.* **1986**, *24*, 1423−1431. (j) Vandenberg, E. J. *Polymer* **1994**, *35*, 4933−4939.

(4) Peretti, K. L.; Ajiro, H.; Cohen, C. T.; Lobkovsky, E. B.; Coates, G. W. *J. Am. Chem. Soc.* **2005**, *127*, 11566−11567.

(5) Ajiro, H.; Peretti, K. L.; Lobkovsky, E. B.; Coates, G. W. *Dalton Trans.* **2009**, 8828−8830.

(6) (a) Hirahata, W.; Thomas, R. M.; Lobkovsky, E. B.; Coates, G. W. *J. Am. Chem. Soc.* **2008**, *130*, 17658−17659. (b) Thomas, R. M.; Widger, P. C. B.; Ahmed, S. M.; Jeske, R. C.; Hirahata, W.; Lobkovsky, E. B.; Coates, G. W. *J. Am. Chem. Soc.* **2010**, *132*, 16520−16525. (c) Widger, P. C. B.; Ahmed, S. M.; Coates, G. W. *Macromolecules* **2011**, *44*, 5666−5670.

(7) Widger, P. C. B.; Ahmed, S. M.; Hirahata, W.; Thomas, R. M.; Lobkovsky, E. B.; Coates, G. W. *Chem. Commun.* **2010**, *46*, 2935−2937.

(8) For recent examples using similar bimetallic catalyst motifs for the copolymerization of epoxides with anhydride and CO_2 comonomers, see: (a) Liu, J.; Bao, Y.-Y.; Liu, Y.; Ren, W.-M.; Lu, X.-B. *Polym. Chem.* **2013**, *4*, 1439−1444. (b) Liu, Y.; Ren, W.-M.; Liu, J.; Lu, X.-B. *Angew. Chem., Int. Ed.* **2013**, *52*, 11594−11598.

(9) (a) Ragone, F.; Poater, A.; Cavallo, L. *J. Am. Chem. Soc.* **2010**, *132*, 4249−4258. (b) Poater, A.; Ragone, F.; Mariz, R.; Dorta, R.; Cavallo, L. *Chem.—Eur. J.* **2010**, *16*, 14348−14353.

(10) (a) Hillier, A. C.; Sommer, W. J.; Yong, B. S.; Petersen, J. L.; Cavallo, L.; Nolan, S. P. *Organometallics* **2003**, *22*, 4322−4326. (b) Viciu, M. S.; Navarro, O.; Germaneau, R. F.; Kelly, R. A.; Sommer, W.; Marion, N.; Stevens, E. D.; Cavallo, L.; Nolan, S. P. *Organometallics* **2004**, *23*, 1629−1635. (c) Poater, A.; Cosenza, B.; Correa, A.; Giudice, S.; Ragone, F.; Scarano, V.; Cavallo, L. *Eur. J. Inorg. Chem.* **2009**, 1759−1766.
(11) Kemper, S.; Hrobárik, P.; Kaupp, M.; Schlörer, N. E. *J. Am. Chem. Soc.* **2009**, *131*, 4172−4173.
(12) Ford, D. D.; Nielsen, L. P. C.; Zuend, S. J.; Musgrave, C. B.; Jacobsen, E. N. *J. Am. Chem. Soc.* **2013**, *135*, 15595−15608.
(13) (a) Coates, G. W. *Chem. Rev.* **2000**, *100*, 1223−1252. (b) Resconi, L.; Cavallo, L.; Fait, A.; Piemontesi, F. *Chem. Rev.* **2000**, *100*, 1253−1346.
(14) (a) Gansäuer, A.; Barchuk, A.; Keller, F.; Schmitt, M.; Grimme, S.; Gerenkamp, M.; Mück-Lichtenfeld, C.; Daasbjerg, K.; Svith, H. *J. Am. Chem. Soc.* **2007**, *129*, 1359−1371. (b) Debuigne, A.; Poli, R.; Jérôme, C.; Jérôme, R.; Detrembleur, C. *Prog. Polym. Sci.* **2009**, *34*, 211−239.
(15) (a) Cavallo, L.; Jacobsen, H. *J. Phys. Chem. A* **2003**, *107*, 5466−5471. (b) Jacobsen, H.; Cavallo, L. *Phys. Chem. Chem. Phys.* **2004**, *6*, 3747−3753.
(16) Bozoglian, F.; Romain, S.; Ertem, M. Z.; Todorova, T. K.; Sens, C.; Mola, J.; Rodriguez, M.; Romero, I.; Benet-Buchholz, J.; Fontrodona, X.; Cramer, C. J.; Gagliardi, L.; Llobet, A. *J. Am. Chem. Soc.* **2009**, *131*, 15176−15187.
(17) (a) Aida, T.; Inoue, S. *J. Am. Chem. Soc.* **1985**, *107*, 1358−1364. (b) Aida, T.; Ishikawa, M.; Inoue, S. *Macromolecules* **1986**, *19*, 8−13. (c) Aida, T.; Inoue, S. *Acc. Chem. Res.* **1996**, *29*, 39−48. (d) Lu, X.-B.; Wang, Y. *Angew. Chem., Int. Ed.* **2004**, *43*, 3574−3577. (e) Darensbourg, D. J.; Billodeaux, D. R. *Inorg. Chem.* **2005**, *44*, 1433−1442. (f) Darensbourg, D. J.; Phelps, A. L. *Inorg. Chem.* **2005**, *44*, 4622−4629. (g) Cohen, C. T.; Chu, T.; Coates, G. W. *J. Am. Chem. Soc.* **2005**, *127*, 10869−10878. (h) Cohen, C. T.; Coates, G. W. *J. Polym. Sci., Part A: Polym. Chem.* **2006**, *44*, 5182−5191. (i) Sugimoto, H.; Kuroda, K. *Macromolecules* **2008**, *41*, 312−317. (j) Nakano, K.; Hashimoto, S.; Nozaki, K. *Chem. Sci.* **2010**, *1*, 369−373. (k) Hosseini Nejad, E.; van Melis, C. G. W.; Vermeer, T. J.; Koning, C. E.; Duchateau, R. *Macromolecules* **2012**, *45*, 1770−1776.
(18) (a) Linde, C.; Arnold, M.; Åkermark, B.; Norrby, P.-O. *Angew. Chem., Int. Ed.* **1997**, *36*, 1723−1725. (b) Strassner, T.; Houk, K. N. *Org. Lett.* **1999**, *1*, 419−422. (c) Cavallo, L.; Jacobsen, H. *Angew. Chem., Int. Ed.* **2000**, *39*, 589−592. (d) Abashkin, Y. G.; Collins, J. R.; Burt, S. K. *Inorg. Chem.* **2001**, *40*, 4040−4048. (e) Linde, C.; Koliaï, N.; Norrby, P.-O.; Åkermark, B. *Chem.—Eur. J.* **2002**, *8*, 2568−2573. (f) Adam, W.; Roschmann, K. J.; Saha-Möller, C. R.; Seebach, D. *J. Am. Chem. Soc.* **2002**, *124*, 5068−5073. (g) Cavallo, L.; Jacobsen, H. *Eur. J. Inorg. Chem.* **2003**, *2003*, 892−902. (h) Cavallo, L.; Jacobsen, H. *Inorg. Chem.* **2004**, *43*, 2175−2182.
(19) (a) Nielsen, L. P. C.; Stevenson, C. P.; Blackmond, D. G.; Jacobsen, E. N. *J. Am. Chem. Soc.* **2004**, *126*, 1360−1362. (b) Nielsen, L. P. C.; Zuend, S. J.; Ford, D. D.; Jacobsen, E. N. *J. Org. Chem.* **2012**, *77*, 2486−2495.
(20) Braune, W.; Okuda, J. *Angew. Chem., Int. Ed.* **2003**, *42*, 64−68.